Proceedings of ESDA 08
9th Biennial ASME Conference on Engineering Systems Design and Analysis
July 7-9, 2008, Haifa, Israel

ESDA2008-59471

DYNAMIC MODELING AND CONTROL OF A PIEZO-ELECTRIC DUAL-STAGE TAPE SERVO ACTUATOR

Uwe Boettcher*, Bart Raeymaekers, Raymond A. de Callafon, Frank E. Talke
Center for Magnetic Recording Research
University of California San Diego
La Jolla, CA 92093-0401
U.S.A.

ABSTRACT

We have implemented the design of a dual-stage actuator tape head for enhanced reduction of lateral tape motion (LTM) disturbance. Our design consists of a conventional voice coil motor (VCM) and a micro-actuator for coarse and fine positioning, respectively. The micro-actuator, which is mounted on the VCM, uses a piezo crystal and allows following LTM up to the kHz regime, while the VCM follows low frequency LTM. Using step response measurements and a realization algorithm, we have created a multi-input discrete-time model of the dual-stage actuator. Based on the model, we designed and implemented a dual-stage controller, using a dual-input single-output approach based on a PQ method. The dual-stage controller controls the position of both actuators and enables an increased track-following bandwidth along with a control signal that is smaller in magnitude than that for a conventional single-stage tape head.

1 INTRODUCTION

State-of-the-art tape drives use a servo mechanism to reject disturbances such as lateral tape motion (LTM). Lateral tape motion is defined as the motion of the tape perpendicular to the tape transport direction. A schematic of a typical tape transport is shown in Fig. 1. The tape moves from the supply reel to the take-up reel at velocity v. Data are written on the tape and read from the tape by the read/write head. The lateral position of the tape head is determined by means of a timing based servo pattern on the magnetic tape [1], and is adjusted by a voice coil motor (VCM) actuator. The read/write head attempts to follow lateral tape motion. However, the magnitude of the control signal is limited by available power in the tape drive, and, thus, the bandwidth of the servo actuator is limited. As a result, high frequency LTM cannot be followed by the servo actuator. This might result in track misregistration, in particular, when narrower tracks are used to accommodate higher storage densities.

To increase the storage capacity on magnetic tapes, it is important to improve the track following servo mechanism. A novel design of a dual-stage actuator tape head was designed by Raeymaekers et al. [2]. A state-of-the-art commercial tape head was modified to include a piezo-based piggyback actuator (PZT). The PZT only actuates the air bearing surface with the read/write elements. This allows increasing the servo bandwidth beyond 500 Hz, which is typically achievable with a VCM actuator while decreasing the magnitude of control signals and allowing frequency separation between the actuators. In this paper we show low bandwidth servo tracking for the VCM; the PZT operates at higher frequencies so that an overall bandwidth improvement can be achieved.

2 EXPERIMENTAL SET-UP

The prototype of our dual-stage actuator tape head, has no timing based servo capability. Instead, the servo mechanism is mimicked by measuring the lateral position of the air bearing surface using a Laser Doppler Vibrometer (LDV). Fig. 2a shows a part of the the experimental set-up in a schematic. The model of the dual-stage actuator G can be seen in Fig. 2 b) were G_{VCM}

*Address all correspondence to this author: uwe@talkelab.ucsd.edu

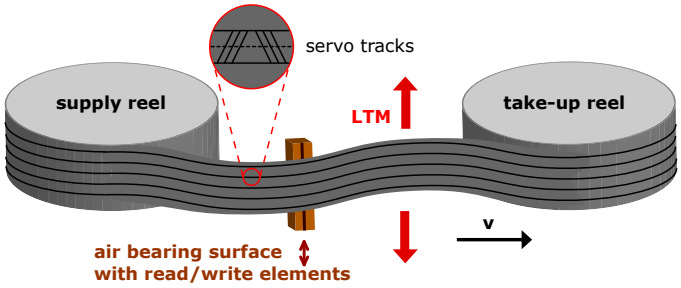

Figure 1. SCHEMATIC OF A TYPICAL TAPE TRANSPORT.

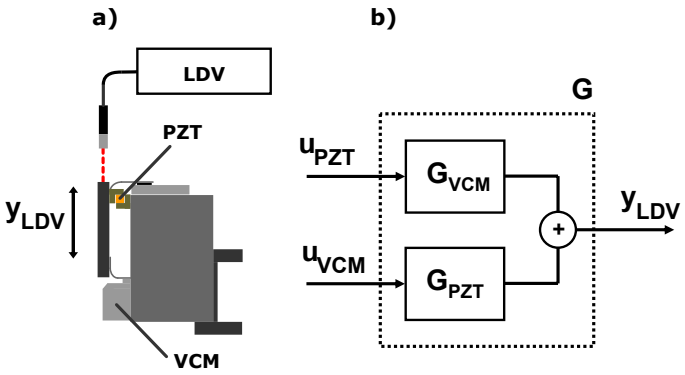

Figure 2. a) SCHEMATIC OF THE DUAL-STAGE ACTUATOR PROTOTYPE b) DUAL-INPUT SINGLE-OUTPUT MODEL.

and G_{PZT} represent the dynamics of the VCM and the PZT, respectively. u_{VCM} and u_{PZT} denote the system input whereas y_{LDV} denotes the system output, which is the position of the air bearing surface.

To achieve the desired lateral displacement of the air bearing surface by using the full range of the D/A convertor, a voltage driver is used to operate the micro-actuator. In addition, a current driver is used to actuate the voice coil motor. We use the velocity output of the LDV to estimate the discrete time models of both micro-actuator and voice coil motor. The data are sampled at 1 MHz to avoid aliasing, and we use averaging (100 times) to average out stochastic noise disturbances.

3 SYSTEM MODELING

The complexity of the mechanical system makes it difficult to use a simplified physical model. Hence, experimental data are used to obtain a discrete time model, using system identification. The Generalized Realization Algorithm (GRA) proposed by de Callafon [3] allows the direct estimation of a discrete time model based on experimental data obtained from input/output relations. As a result, one obtains a good approximation of the matrices

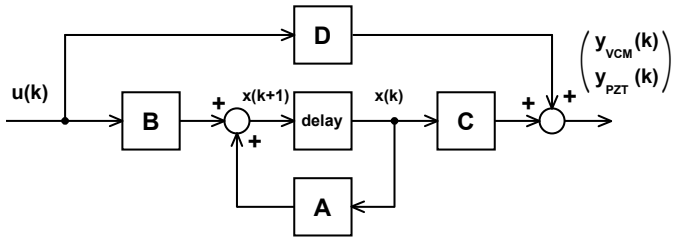

Figure 3. STANDARD FORM OF A STATE SPACE REALIZATION

A,B and C of a standard state space realization, illustrated in Fig. 3. Here, $u(k)$ represents the system input, while $y_{\mathrm{VCM}}(k)$ and $y_{\mathrm{PZT}}(k)$ represent the system output. To estimate a model of the VCM and the micro-actuator, we have measured the response to a 1 V step-function. The measurement data are stored in a $2N \times N$ block Hankel Matrix $\mathbf{Y}$

$$\mathbf{Y} = \begin{bmatrix} y_{\mathrm{v}}(1) & y_{\mathrm{v}}(2) & \cdots & y_{\mathrm{v}}(N) \\ y_{\mathrm{p}}(1) & y_{\mathrm{p}}(2) & \cdots & y_{\mathrm{p}}(N) \\ y_{\mathrm{v}}(2) & y_{\mathrm{v}}(3) & \cdots & y_{\mathrm{v}}(N+1) \\ y_{\mathrm{p}}(2) & y_{\mathrm{p}}(3) & \cdots & y_{\mathrm{p}}(N+1) \\ \vdots & \vdots & \vdots & \vdots \\ y_{\mathrm{v}}(N) & y_{\mathrm{v}}(N+1) & \cdots & y_{\mathrm{v}}(2N-1) \\ y_{\mathrm{p}}(N) & y_{\mathrm{p}}(N+1) & \cdots & y_{\mathrm{p}}(2N-1) \end{bmatrix} \tag{1}$$

where N denotes the number of data points taken into account for each measurement.The vectors y_{v} and y_{p} denote the measured step response of the VCM and the PZT, respectively.

The GRA is related to the Ho-Kalman algorithm [4] which uses the decomposition of a Hankel matrix that contains the Markov parameters (impulse response terms) of the system. Instead we use step response measurements. For a unit voltage step input and a two-dimensional output, the modeling algorithm [3] works as follows. The input/output relationship can be written in a Hankel matrix representation

$$\mathbf{R} = \mathbf{Y} - \mathbf{E} \tag{2}$$

where $\mathbf{Y}$ is the output matrix described in (1) and $\mathbf{E}$ is the error matrix. The error matrix is a row-wise listing of output signals in block structure.

$$\mathbf{E} = \begin{bmatrix} y_{\mathrm{v}}(1) & \cdots & y_{\mathrm{v}}(1) \\ y_{\mathrm{p}}(1) & \cdots & y_{\mathrm{p}}(1) \\ \vdots & \vdots & \vdots \\ y_{\mathrm{v}}(N) & \cdots & y_{\mathrm{v}}(N) \\ y_{\mathrm{p}}(N) & \cdots & y_{\mathrm{p}}(N) \end{bmatrix} \tag{3}$$

The matrix $\mathbf{R}$ is decomposed into a $2N \times n$ matrix $\mathbf{R_1}$ and an $N \times n$ matrix $\mathbf{R_2}$, by using singular value decomposition. This decomposition enables choosing the rank n, and, thus, the order of the estimated model. The matrix $\mathbf{R}$ can be also described as

$$\bar{\mathbf{R}} = \bar{\mathbf{Y}} - \bar{\mathbf{E}} = \mathbf{R_1 A R_2} \tag{4}$$

Here, $\bar{\mathbf{Y}}$ is the the shifted version of $\mathbf{Y}$ given in (5)

$$\bar{\mathbf{Y}} = \begin{bmatrix} y_v(2) & y_v(3) & \cdots & y_v(N+1) \\ y_p(2) & y_p(3) & \cdots & y_p(N+1) \\ y_v(3) & y_v(4) & \cdots & y_v(N+2) \\ y_p(3) & y_p(4) & \cdots & y_p(N+2) \\ \vdots & \vdots & \vdots & \vdots \\ y_v(N+1) & y_v(N+2) & \cdots & y_v(2N) \\ y_p(N+1) & y_p(N+2) & \cdots & y_p(2N) \end{bmatrix} \tag{5}$$

$\bar{\mathbf{R}}$ and $\bar{\mathbf{E}}$ denote the shifted version of $\mathbf{R}$ and $\mathbf{E}$, analogous to $\mathbf{Y}$ and $\bar{\mathbf{Y}}$. When $\mathbf{R_1}$, $\mathbf{R_2}$ and $\bar{\mathbf{R}}$ are known, the state space matrix $\mathbf{A}$ can be estimated. The input matrix $\mathbf{B}$ and the output matrix $\mathbf{C}$ can then be described as the first column of $\mathbf{R_2}$ and the first two rows of $\mathbf{R_1}$, respectively. Based on a plot of the singular values of $\mathbf{R}$ and a model validation, the model order was chosen to be high enough to capture most of the system dynamics of both, the VCM and the PZT.

The estimated 30^{th} order model is validated in two different ways. First, the model is used to simulate an input step which is compared to the actual step response measurement. The result of this time domain validation is illustrated in Fig. 4 and shows excellent agreement between the simulated and measured step response data. Fig. 4 a) shows the results for the voice coil motor and Fig. 4 b) shows the results for the micro-actuator.

Secondly, the model is validated in the frequency domain, by measuring the frequency response function of both the VCM and micro-actuator with a dynamic signal analyzer. The result of this frequency domain validation is shown in Fig. 5. Fig. 5 a) shows the results for the voice coil motor and Fig. 5 b) shows the results for the micro-actuator.

From Fig. 5, we observe good agreement between the measured FRF and the estimated model. The model captures almost all high frequency resonance modes. Based on several measurements with different fixtures for the tape head, we postulate that the small resonance mode at 500Hz corresponds to the fixture of the tape head. Furthermore, we believe that the resonance mode at 2kHz corresponds to the eigenfrequency of the micro-actuator (the spring-mass-damper system of the leaf springs and the air bearing surface).

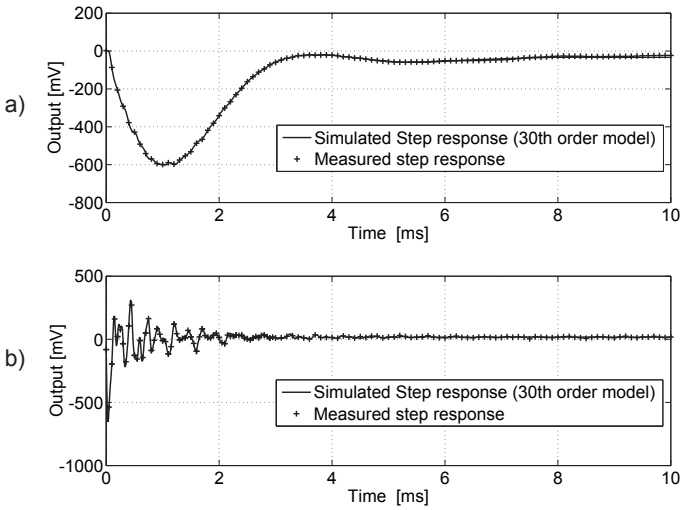

Figure 4. TIME DOMAIN VALIDATION a) VOICE COIL MOTOR AND b) MICRO-ACTUATOR

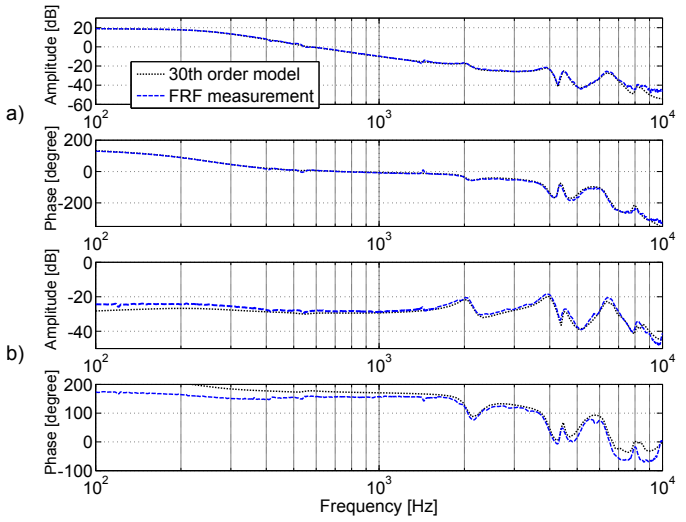

Figure 5. FREQUENCY DOMAIN VALIDATION a) VOICE COIL MOTOR AND b) MICRO-ACTUATOR

4 DUAL-STAGE CONTROLLER DESIGN

Dual-stage controllers are well-known in hard disk drive technology [5]. However, in the design of our dual-stage actuator tape head, the relative motion between the two actuators is unknown, and we only use one position measurement to determine the lateral position of the air bearing surface. Thus, the system is considered as a dual-input single-output system (DISO).

The servo control structure for the dual-stage actuator tape head is shown in Fig. 6. The signal e is the difference between the

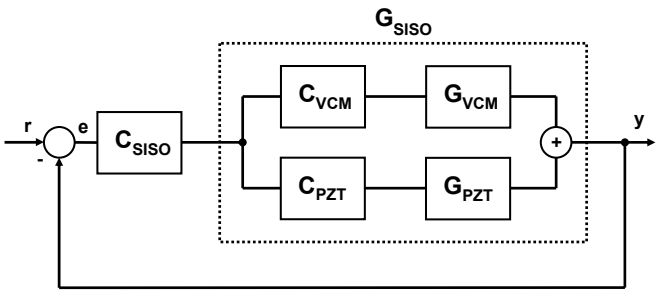

Figure 6. DUAL-STAGE ACTUATOR TAPE HEAD CONTROL DESIGN

desired lateral position of the tape head r and the actual lateral position of the tape head y (controller output). The controller design is based on the PQ method which was first proposed in [6] and applied to a dual stage controller in hard disk drives in [7]. The PQ method allows to decompose a DISO system into two SISO systems. C_{VCM} and C_{PZT} are the VCM and micro-actuator controllers. G_{VCM} and G_{PZT} represent the dynamics of both actuators.

The VCM controller C_{VCM} is given in (6). It contains an integrator to remove the steady-state error and reject disturbances. A second order lead compensator increases the phase margin and ensures stability in the feedback loop. The micro-actuator controller given in (7) is designed as a high pass filter, since it only needs to respond to LTM frequencies above several hundred Hertz. Figure 7 a) shows the Bode diagram of the VCM, while Fig. 7 b) shows the Bode diagram of the micro-actuator.

$$C_{\mathrm{VCM}} = \frac{(z-0.8966)}{(z-0.999)} \cdot \frac{(z-0.9687)^2}{(z^2-1.31z+0.6289)} \tag{6}$$

$$C_{\mathrm{PZT}} = 7.43 \cdot \frac{(z-0.999)}{(z-0.7789)} \tag{7}$$

The controller C_{SISO} handles the closed-loop stability and performance of the overall system. To increase the bandwidth to the maximum achievable for this actuator, several notch filters were used to cancel out high frequency resonance modes. Figure 8 shows the open loop transfer function of both actuators C_{VCM} and C_{PZT}. The transfer function of the overall system $C_{\mathrm{SISO}} \cdot G_{\mathrm{SISO}}$ can be obtained by summing the transfer functions of the VCM and the micro-actuator, i.e., $C_{\mathrm{SISO}} \cdot G_{\mathrm{SISO}} = C_{\mathrm{SISO}} \cdot C_{\mathrm{VCM}} \cdot G_{\mathrm{VCM}} + C_{\mathrm{SISO}} \cdot C_{\mathrm{PZT}} \cdot G_{\mathrm{PZT}}$

We have compared the performance of our dual-stage controller to a single-stage controller C_{ss}, which only uses the voice

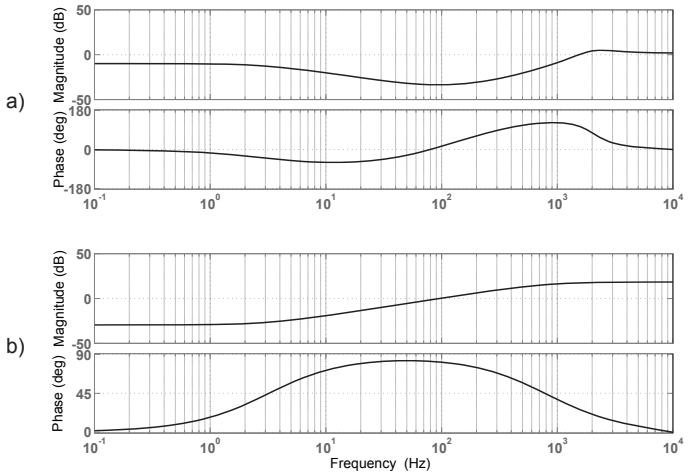

Figure 7. BODE PLOT OF a) C_{VCM} AND b) C_{PZT}

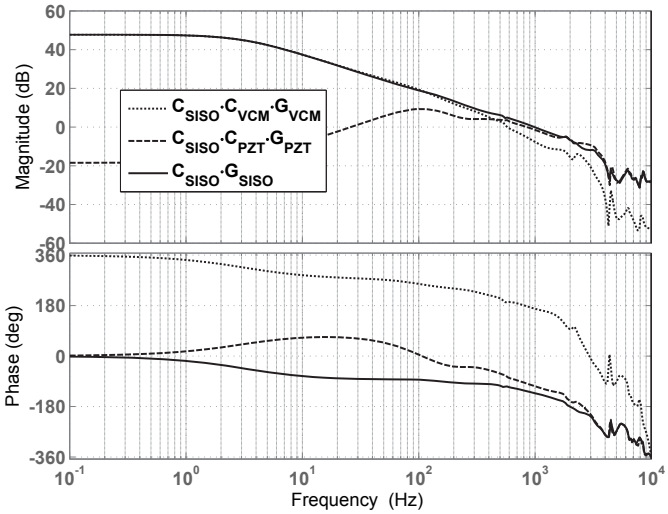

Figure 8. OPEN LOOP TRANSFER FUNCTIONS

coil motor. C_{ss} uses a notch filter at 2 kHz. The sensitivity function (error rejection function) of both the single-stage and dual-stage controller are shown in Fig. 9.

From Fig. 9, we observe that the single-stage controller design has a better disturbance rejection at frequencies below 240 Hz, while the dual-stage controller has a better disturbance rejection above that frequency. The system parameters for both designs are listed in Table 1.

The closed loop bandwidth of the dual-stage design shows an improvement of approximately 25% compared to the single-stage design. However, the main advantage of the dual-stage versus the single-stage controller can be seen in Fig. 10. Figure 10

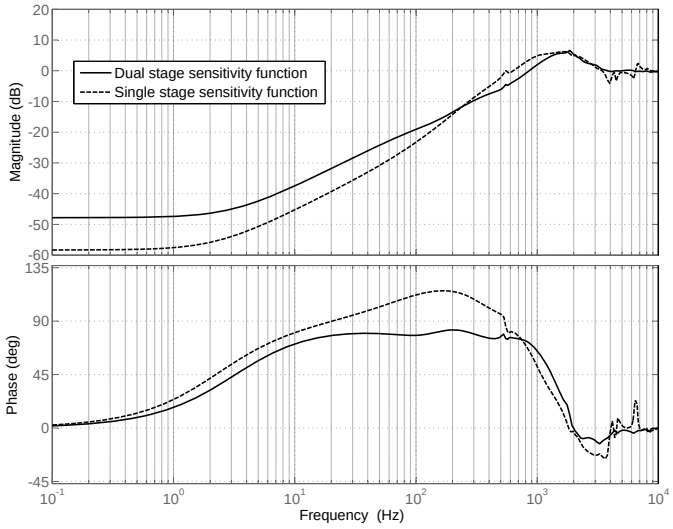

Figure 9. CLOSED LOOP TRANSFER FUNCTION AND SENSITIVITY FUNCTION OF SINGLE-STAGE AND DUAL-STAGE DESIGN

Table 1. SYSTEM PARAMETERS

	Single-stage	**Dual-stage**
gain margin	6dB	6.8 dB
phase margin	42 degrees	48 degrees
overshoot	33%	21%
5% settling time	1.1 s	0.8 s
closed loop bandwidth	≈ 800Hz	≈ 1kHz

a) shows the lateral position of the tape head, while Fig. 10 b) shows the magnitude of the control signal, for a step response. The solid line and the dashed line represent the dual-stage and single-stage controller, respectively. The dotted line shows the reference signal r, i.e., the desired lateral position of the tape head.

The magnitude of the control signal of the VCM in the dual-stage design is approximately three times smaller than in the single-stage design, for the same displacement. Hence, the dual-stage controller can reject disturbances with larger amplitudes than the single-stage controller, since the available power in a tape drive is limited.

5 CONTROLLER IMPLEMENTATION

The dual-stage controller was implemented in the dual-stage actuator tape head prototype. We have applied a 100 Hz square wave reference signal of 0.1 V amplitude. Figure 11 shows

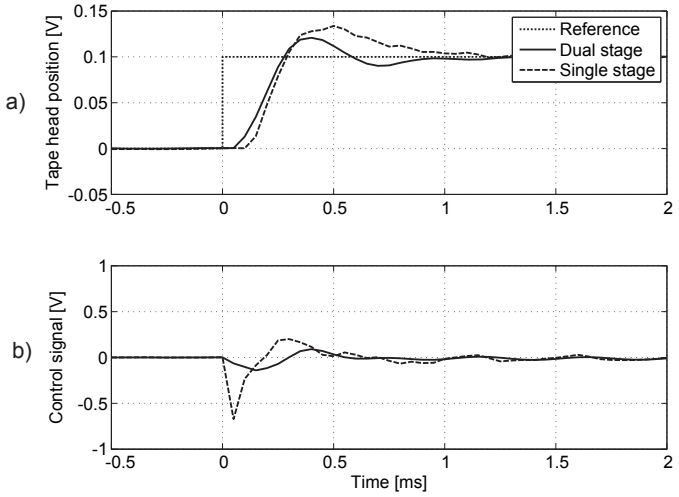

Figure 10. SIMULATED STEP RESPONSE FOR DUAL-STAGE AND SINGLE-STAGE CONTROL DESIGN

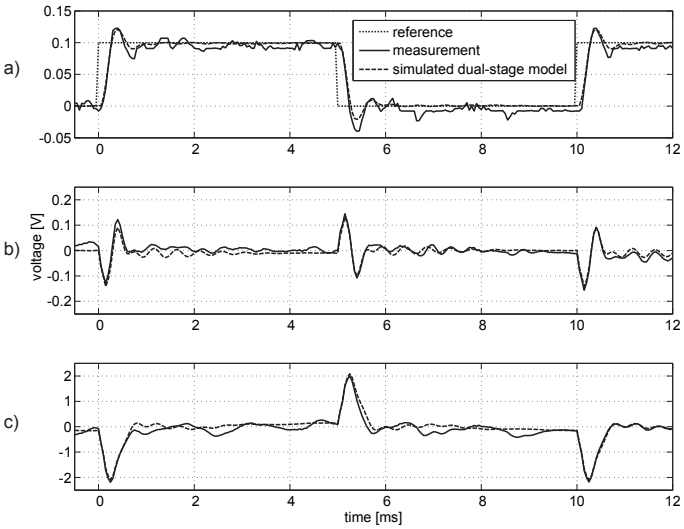

Figure 11. IMPLEMENTED CONTROLLER

the results. Figure 11 a) shows the lateral tape head position; Fig. 11 b) shows the control signal for the voice coil motor; Fig. 11 c) shows the control signal for the micro-actuator.

From Fig. 11, we observe that the dual-stage controller settles the lateral position of the tape head to the desired (reference) position within less than 1 ms. The simulated output signal and the two simulated control signals are in very good agreement with the measurements. To illustrate the frequency separation obtained with the dual-stage controller, we have simulated the individual displacement of both actuators. The results are shown in Fig. 12. We observe that the VCM moves to the desired posi-

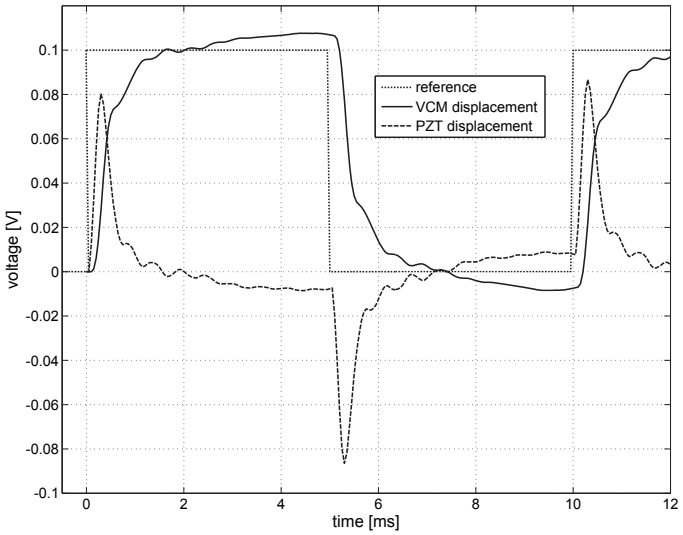

Figure 12. SIMULATED CONTROLLER

tion slowly, while the micro-actuator acts fast and moves back to its zero position, since there is no DC component in the control signal for the micro-actuator.

6 DISCUSSION AND CONCLUSION

A dual-stage controller for a dual-stage actuator tape head has been designed and implemented. The dual-stage design uses less control energy than a comparable single-stage design. Thus, it enables rejection of disturbances with larger amplitudes. The estimated model shows an excellent agreement with the measured results.

Furthermore, we have achieved an improvement in the closed loop bandwidth. However, since the first peak in the FRF of the micro-actuator is close to the maximum achievable closed-loop bandwidth of the VCM, this improvement is relatively small. The mechanical design of the prototype could be altered to yield a stiffer second stage. A higher stiffness would move some of the low frequency resonance modes in the frequency response function to a higher frequency, and, thus, would allow a larger closed loop bandwidth.

REFERENCES

[1] R.C. Barrett, E.H. Klaassen, T.R. Albrecht, G.A. Jacquette,J.H. Eaton *1998 Timing-based track-following servo for linear tape systems* IEEE Trans. Magn. 34(4): 1872 - 1877 Part 1

[2] B. Raeymaekers, M.R. Graham, R.A. de Callafon, F.E. Talke *2007 Design of a dual stage actuator tape head width high bandwidth track-following capability* Proceedings of ASME Information Storage and Processing Systems Conference, Santa Clara, CA, USA

[3] R.A. de Callafon *2003 Estimating parameters in a lumped parameter system with first principle modeling and dynamic experiments* Proceedings of 13th IFAC Symposium on System Identification, 1613 - 1618, Rotterdam, the Netherlands

[4] R.E. Kalman, B.L. Ho *1966 Effective construction of linear state-variable models from input/output functions* Regelungstechnik 14:545 548

[5] T. Semba, T. Hirano, J. Hongt, L. Fan, L. *1999 Dual-stage servo controller for HDD using MEMS microactuator* IEEE Trans. Magn. 35(5): 2271 - 2273

[6] S.J. Schroeck, W.C. Messner *1999 On controller design for linear time-invariant dual-input single-output systems* Proceedings of the American Control Conference, San Diego, CA, USA

[7] M. Graham, R.J.M. Oosterbosch,R.A. de Callafon *2005 Fixed order PQ-control design method for dual stage instrumented suspension* IFAC Congress, Praha, Czech Republic